Phosphorylation of STEF/Tiam2 by protein kinase A is critical for Rac1 activation and neurite outgrowth in dibutyryl cAMP–treated PC12D cells

Akihiro Goto[a], Mikio Hoshino[b], Michiyuki Matsuda[a], and Takeshi Nakamura[a,c]
[a]Laboratory of Bioimaging and Cell Signaling, Graduate School of Biostudies, Kyoto University, Sakyo-ku, Kyoto, Japan; [b]Department of Biochemistry and Cellular Biology, National Institute of Neuroscience, NCNP, Kodaira, Tokyo, Japan; [c]Division of Biosignaling, Research Institute for Biological Sciences, Tokyo University of Science, Noda, Chiba, Japan

ABSTRACT **The second messenger cAMP plays a pivotal role in neurite/axon growth and guidance, but its downstream pathways leading to the regulation of Rho GTPases, centrally implicated in neuronal morphogenesis, remain elusive. We examined spatiotemporal changes in Rac1 and Cdc42 activity and phosphatidylinositol 3,4,5-triphosphate (PIP_3) concentration in dibutyryl cAMP (dbcAMP)-treated PC12D cells using Förster resonance energy transfer–based biosensors. During a 30-min incubation with dbcAMP, Rac1 activity gradually increased throughout the cells and remained at its maximal level. There was no change in PIP_3 concentration. After a 5-h incubation with dbcAMP, Rac1 and Cdc42 were activated at the protruding tips of neurites without PIP_3 accumulation. dbcAMP-induced Rac1 activation was principally mediated by protein kinase A (PKA) and Sif- and Tiam1-like exchange factor (STEF)/Tiam2. STEF depletion drastically reduced dbcAMP-induced neurite outgrowth. PKA phosphorylates STEF at three residues (Thr-749, Ser-782, Ser-1562); Thr-749 phosphorylation was critical for dbcAMP-induced Rac1 activation and neurite extension. During dbcAMP-induced neurite outgrowth, PKA activation at the plasma membrane became localized to neurite tips; this localization may contribute to local Rac1 activation at the same neurite tips. Considering the critical role of Rac1 in neuronal morphogenesis, the PKA—STEF–Rac1 pathway may play a crucial role in cytoskeletal regulation during neurite/axon outgrowth and guidance, which depend on cAMP signals.**

Monitoring Editor
Kozo Kaibuchi
Nagoya University

Received: Sep 22, 2010
Revised: Feb 17, 2011
Accepted: Mar 21, 2011

This article was published online ahead of print in MBoC in Press (http://www.molbiolcell.org/cgi/doi/10.1091/mbc.E10-09-0783) on April 1, 2011.

Address correspondence to: Takeshi Nakamura (tnakamr@rs.noda.tus.ac.jp).

Abbreviations used: 007, 8-para-chloro-phenyl-thio-2′-O-methyl-cAMP; 6-Bnz-cAMP, N^6-benzoyladenosine-3′,5′-cyclical monophosphate; AKAP, A kinase anchoring protein; CFP ; dbcAMP, dibutyryl cAMP; Epac, exchange protein directly activated by cAMP; FRET, Förster resonance energy transfer; GEF, guanine nucleotide exchange factor; NGF, nerve growth factor; PACAP, pituitary adenylate cyclase-activating polypeptide; PI3-kinase, phosphatidylinositol 3-kinase; PIP_3, phosphatidylinositol 3,4,5-triphosphate; PKAprotein kinase A; PRKACA, rat PKA catalytic subunit α; PRKACB, rat PKA catalytic subunit β; shRNA, short-hairpin RNA; STEF, Sif and Tiam1-like exchange factor; TSS, Tiam1-SIF-STEF homology.

INTRODUCTION

Neurite/axon outgrowth is essential for both the initial wiring of neuronal networks during development and the regeneration of synaptic connections in the injured adult nervous system. cAMP, which exhibits profound effects on growth cone motility and guidance (Zheng *et al*., 1994; Piper *et al*., 2007), transmits signals primarily through protein kinase A (PKA) and exchanges protein directly activated by cAMP (exchange protein directly activated by cAMP [Epac]/cAMP-guanine nucleotide exchange factor [GEF]) (Fimia and Sassone-Corsi, 2001; Bos, 2006). Previous studies have linked elevated cAMP signaling with enhanced neurite elongation (Richter-Landsberg and Jastorff, 1986; Rydel and Greene, 1988). An increase in cAMP levels converted the inhibition of neurite outgrowth and repulsive turning of growth cones by myelin-associated inhibitors

toward neurite extension and attraction (Song *et al.*, 1998; Cai *et al.*, 1999). Furthermore, in vivo studies have shown that cAMP elevation promoted axonal regeneration (Neumann *et al.*, 2002; Qiu *et al.*, 2002) and an odorant receptor-derived cAMP signal determined the target destination of olfactory sensory networks (Imai *et al.*, 2006).

Rho-family GTPases (RhoA, Rac1, and Cdc42), which regulate actin dynamics in a range of cellular functions (Van Aelst and D'Souza-Schorey, 1997; Hall, 1998), also play central roles in neuronal morphogenesis, including axon growth and guidance (Luo, 2000; Heasman and Ridley, 2008). Recent studies have revealed signaling pathways from various neuritogenic factors and guidance cues to Rho-family GTPases (Heasman and Ridley, 2008; Hall and Lalli, 2010). However, the mechanisms that transduce cAMP signals for the regulation of Rho GTPases during axon growth and guidance are largely unknown, except for the report that PKA facilitated neurite formation by inhibiting RhoA through direct phosphorylation of Ser-188 (Dong *et al.*, 1998). Furthermore, there is only limited information about when and where Rho GTPases are activated in neuronal cells following cAMP elevation.

Förster resonance energy transfer (FRET)-based biosensors enable us to visualize a variety of signaling events, including G protein activation and change in phosphatidylinositol concentration in living cells (Miyawaki, 2003; Nakamura and Matsuda, 2009). Using FRET-based biosensors, we have previously shown that Rac1, Cdc42, and phosphatidylinositol 3-kinase (PI3-kinase) are locally and repetitively activated at protruding sites following their transient activation in broad areas of the cell periphery during nerve growth factor (NGF)-induced neurite outgrowth in PC12 cells (Aoki *et al.*, 2004, 2005). On the basis of these findings, we have demonstrated that NGF promotes the cycling of a positive feedback loop composed of PI3-kinase, Vav2/Vav3, Rac1/Cdc42, and the actin cytoskeleton at neurite tips (Aoki *et al.*, 2005).

In this study, we first examined spatiotemporal changes in Rac1/Cdc42 activity and phosphatidylinositol 3,4,5-triphosphate (PIP_3) concentration in dibutyryl cAMP (dbcAMP)-treated PC12D cells using FRET-based biosensors. Rac1 activity was gradually increased throughout the cells during the initial 10 min after dbcAMP addition and kept its maximal level during the succeeding 20 min. This Rac1 activation did not accompany any change of PIP_3 concentration. After several hours of incubation with dbcAMP, Rac1 and Cdc42 were locally activated at the protruding tips of neurites. We have shown that dbcAMP-induced Rac1 activation was principally mediated by PKA and Sif- and Tiam1-like exchange factor (STEF)/Tiam2. STEF depletion severely reduced dbcAMP-induced neurite outgrowth. PKA could phosphorylate STEF at three residues (Thr-749, Ser-782, S-1562), and Thr-749 phosphorylation was important for dbcAMP-induced Rac1 activation and neurite extension. Considering the critical role of Rac1 in neuronal morphogenesis, the PKA—STEF–Rac1 pathway shown here may play a crucial role in cytoskeletal regulation during neurite/axon outgrowth and guidance, which depend on cAMP signals.

RESULTS

Early response of Rac1 and Cdc42 activity and PIP_3 concentration to dbcAMP treatment is different from the early response to NGF stimulation in PC12D cells

Using FRET-based biosensors, we examined spatiotemporal changes in Rac1 and Cdc42 activity and PIP_3 concentration for 30 min following dbcAMP treatment in PC12D cells (Figure 1A). Rac1 activity was gradually increased throughout the cells during the initial 10 min after dbcAMP addition, and it maintained its maximal level during the succeeding 20 min (Figure 1B, left) and longer. The activity of Cdc42 linearly decreased during the initial 10 min and maintained its lowest level during the succeeding 20 min (Figure 1B, middle). Throughout the 30 min after dbcAMP addition, we did not find any significant changes in PIP_3 level (Figure 1B, right); this result is consistent with our result that Rac1 activation following dbcAMP treatment was not inhibited by LY294002 treatment (Supplemental Figure 1A). These results showed a clear contrast with the local and repetitive Rac1 and Cdc42 activation and PIP_3 accumulation at the protruding sites following an initial transient increase in NGF-treated cells (Figure 1B, blue lines; Aoki *et al.*, 2004, 2005).

Rac1 and Cdc42 are locally activated at the tips of dbcAMP-induced neurites

Our previous observation that local and repetitive Rac1 and Cdc42 activation and PIP_3 accumulation were also observed at the protruding tips of neurites 5 h or 1 d after NGF stimulation (Aoki *et al.*, 2004 and unpublished results) prompted us to examine the spatiotemporal changes in Rac1 and Cdc42 activity and PIP_3 concentration for 5 h after dbcAMP addition. Figure 1C shows that Rac1 and Cdc42 were locally activated at the neurite tips without any PIP_3 accumulation in dbcAMP-treated PC12D cells. We quantified this activity localization in neurite tips by using line-scanned data and linear fitting. The activity of Rac1 and Cdc42, but not PIP_3 concentration, showed a significant positive gradient in neurite tips (Figure 1D). This result is consistent with our result that LY294002 treatment did not inhibit dbcAMP-induced neurite outgrowth (Supplemental Figure 1B).

Although local activation of both Rac1 and Cdc42 was observed in common at the tips of NGF- and dbcAMP-induced neurites, there was a clear difference in the mode of activation: Compared with the frequently alternating activation and inactivation at NGF-induced neurite tips (Aoki *et al.*, 2004), the tips of dbcAMP-induced neurites showed a sustained Rac1 and Cdc42 activation (Supplemental Videos 1 and 2).

Next we compared the mode of morphological change between NGF-induced and dbcAMP-induced neurites. NGF-induced neurites repeated a rapid cycle of extension and retraction as expected from the mode of Rac1 and Cdc42 activation (Figure 2A, left; Supplemental Video 3), whereas dbcAMP-induced neurites extended continuously (Figure 2A, right; Supplemental Video 4), consistent with the sustained Rac1 and Cdc42 activation at the tips of dbcAMP-induced protrusions. To quantify the amplitude of extension/retraction of neurite lengths, the deviation from the five-point average was calculated for each time-point. Thereafter the sum of the absolute value of the deviation was obtained for each sample. The mean accumulated deviation from the five-point average in dbcAMP-treated cells was half of that in NGF-stimulated cells (Figure 2B).

dbcAMP-induced Rac1 activation is principally mediated by PKA

To clarify the mechanism of dbcAMP-induced Rac1 activation, we first examined the effects of the PKA-specific cAMP analogue 6-Bnz-cAMP (Christensen *et al.*, 2003) and the Epac-specific cAMP analogue 007 (Enserink *et al.*, 2002) on Rac1 activation. We confirmed the specificity of 6-Bnz-cAMP and 007 using FRET-based biosensors (Supplemental Figure 2). The time-course of Rac1 activation within 30 min after 6-Bnz-cAMP treatment was similar to that in dbcAMP-treated cells (Figure 3A, left). The average of the highest values of Rac1 activation following 6-Bnz-cAMP treatment was 86% of that in dbcAMP-treated cells (Figure 3A, right). In contrast, the average of

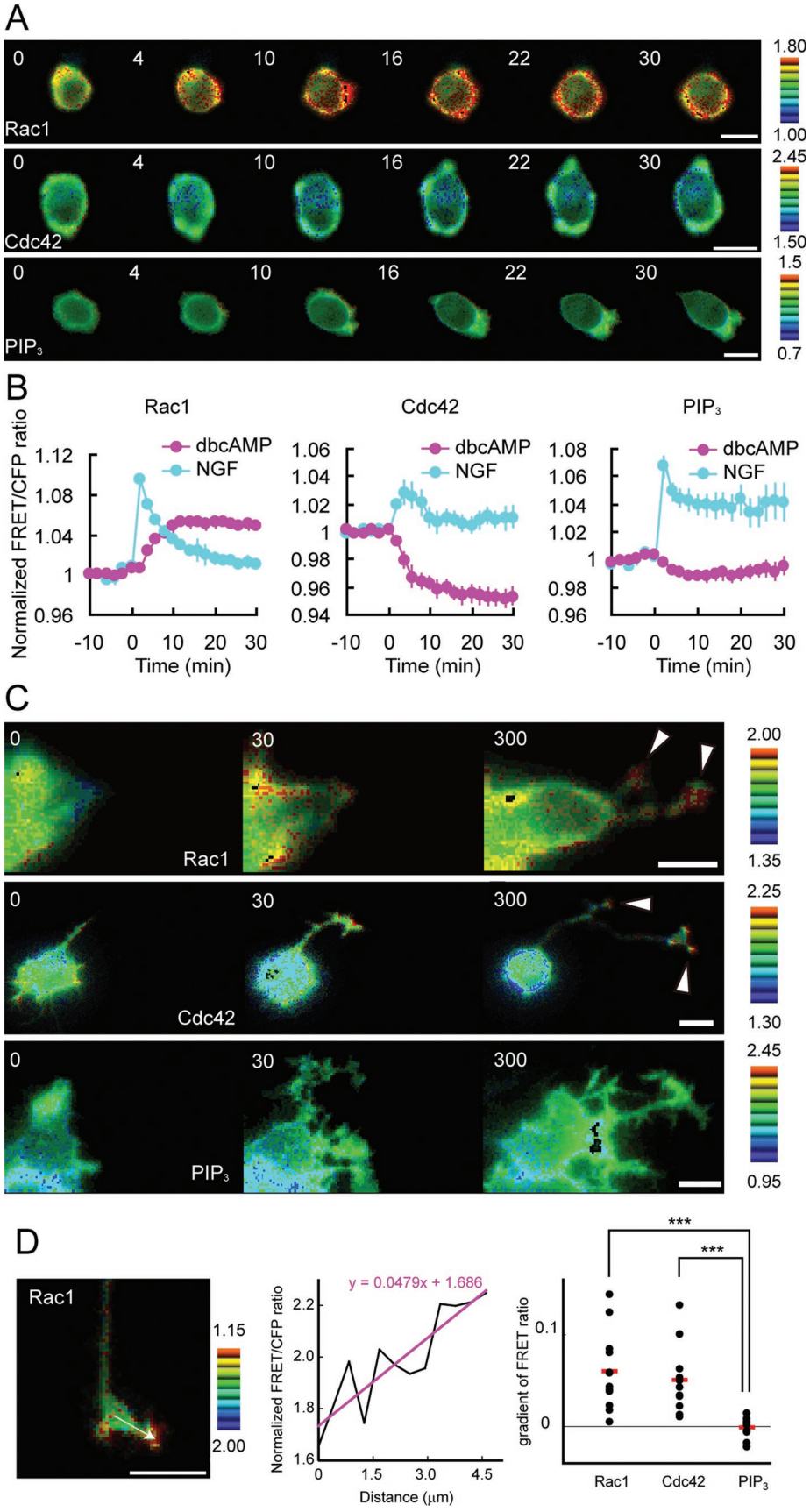

FIGURE 1: Spatiotemporal changes in Rac1 and Cdc42 activity and PIP_3 concentration following dbcAMP treatment. (A and B) PC12D cells expressing Raichu-Rac1, Raichu-Cdc42, or Pippi-PIP_3 were starved for 2 h and then treated with 1 mM dbcAMP. Images were obtained every 2 min for 30 min after dbcAMP addition. (A) Representative ratio images of FRET/CFP at the indicated time points (in min) after dbcAMP addition are shown in the intensity-modulated display mode. In the intensity-modulated display mode, eight colors from red to blue are used to represent the FRET/CFP ratio, with the intensity of each color indicating the mean intensity of FRET and CFP. The upper and lower limits of the ratio images are shown on the right. Bars, 10 μm. (B) The mean FRET/CFP ratios averaged over the whole cell are expressed by measuring the relative increase compared with the reference value, which was averaged over10 min before dbcAMP addition. The number of experiments was as follows: Rac1 (n = 20), Cdc42 (n = 9), PIP_3 (n = 21). Error bars show the SE. (C) The long-term response of Rac1 and Cdc42 activity and PIP_3 concentration following dbcAMP treatment was examined as described for (A). Images were obtained every 5 min for 5 h after dbcAMP addition. Representative ratio images of FRET/CFP at the indicated time points (in min) after dbcAMP addition are shown as described for (A). Bars, 10 μm. (D) Images were obtained every 5 min for 1 h after a 1-d treatment with dbcAMP. A gradient of normalized FRET/CFP ratio measured by line scanning in neurite tips (left) was obtained by linear fitting (middle) and plotted for Rac1 and Cdc42 activity and PIP_3 concentration (right). The number of experiments was as follows: Rac1 (n = 12), Cdc42 (n = 11), PIP_3 (n = 10). Red bars represent averages. The symbols indicate the results of a Student's *t* test analysis (***$p < 0.001$).

the highest values of Rac1 activation following 007 treatment was only 13% of that in dbcAMP-treated cells (Figure 3A, right).

The primary role of PKA in dbcAMP-induced Rac1 activation was further confirmed by targeted depletion of PKA and Epac by RNA interference. We used an shRNA expression vector containing the pac gene to allow selection of shRNA-expressing cells with puromycin. Two isoforms of the catalytic subunits of PKA (α and β), PRKACA and PRKACB, respectively, are expressed in neuronal cells. In PRKACA shRNA–expressing cells, 80% of endogenous PRKACA was depleted (Supplemental Figure 3A). In PRKACB shRNA–expressing cells, quantitative real-time RT-PCR analysis showed a 90% reduction in the level of endogenous PRKACB mRNA (Supplemental Figure 3A). The silencing effect of PRKACB shRNA was confirmed by the efficient depletion of exogenous PRKACB protein (Supplemental Figure 3A). Epac

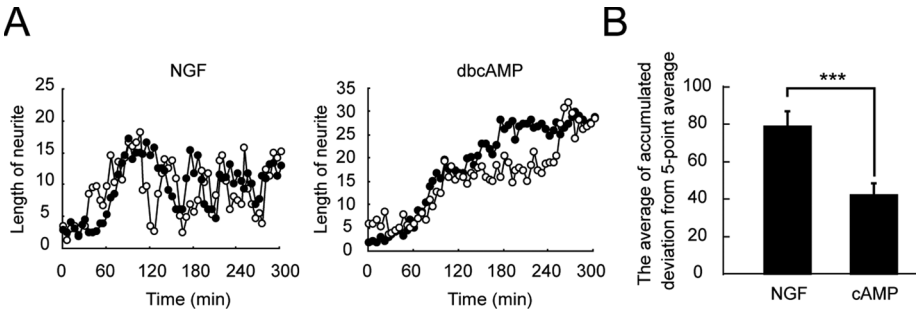

FIGURE 2: Different modes of neurite outgrowth in NGF- and dbcAMP-treated PC12D cells. PC12D cells were treated with NGF or dbcAMP and imaged every 5 min for 5 h. The length of the longest neurites was measured for each image. The number of experiments was as follows: NGF (n = 12), dbcAMP (n = 12). (A) Two representative time-dependent changes in neurite length are shown for NGF-treated cells (left) and dbcAMP-treated cells (right). (B) The bar graph shows the average of accumulated deviation from the five-point average, with SE. The symbol indicates the result of a Student's *t* test (***$p < 0.001$).

has two isoforms, Epac1 and Epac2. In Epac1 shRNA–expressing cells, real-time RT-PCR analysis showed a 60% reduction in the level of the endogenous transcript (Supplemental Figure 3B). In Epac2 shRNA–expressing cells, 90% of endogenous Epac2 protein was depleted (Supplemental Figure 3B).

Depletion of the catalytic subunits of PKA markedly reduced dbcAMP-induced Rac1 activation in PC12D cells (Figure 3B). The average of the highest values of Rac1 activation in the PRKACA- and PRKACB-depleted cells was 33% of that in control cells. In contrast, the average of the highest values of Rac1 activation was comparable between control and Epac-depleted cells. Taken together, dbcAMP-induced Rac1 activation is principally mediated by PKA in PC12D cells.

Depletion of STEF abolishes dbcAMP-induced activation of Rac1

Next we tried to identify the GEFs responsible for dbcAMP-dependent Rac1 activation. Rac1, but not Cdc42, was activated shortly after dbcAMP addition (Figure 1, A and B). Candidates for Rac1-specific GEFs that are expressed in neuronal tissues are Tiam1, STEF, Dock180, Dock3, Dock4, and kalirin. We did not suspect the Dock family members because their activation is thought to be mainly dependent on a RhoG/Elmo/Dock interaction (Cote and Vuori, 2007) and the expression level of RhoG in naïve PC12 cells is low and increases only during differentiation (Katoh *et al.*, 2000). We tentatively excluded kalirin because its level is low during initial neural development and increases gradually (McPherson *et al.*, 2002), although a role for the kalirin-RhoG pathway in NGF-induced neurite outgrowth has been reported in PC12 cells (Chakrabarti *et al.*, 2005). Tiam1 and STEF shRNAs efficiently reduced the amount of endogenous Tiam1 and STEF proteins, respectively (Supplemental Figure 4).

Depletion of STEF almost completely abolished dbcAMP-induced Rac1 activation (Figure 4). Knockdown of Tiam1, a close homolog of STEF, reduced dbcAMP-induced Rac1 activation by half. Depletion of Vav2/Vav3, which has been shown to primarily mediate Rac1 and Cdc42 activation in NGF-treated PC12 cells (Aoki *et al.*, 2005), did not affect Rac1 activation in dbcAMP-treated PC12D cells. We further examined the role of STEF in cAMP-induced Rac1 activation using a physiological ligand. Pituitary adenylate cyclase-activating polypeptide (PACAP) binds to its G-protein–coupled receptors, which in turn activate adenylate cyclase and promote cAMP generation (Somogyvari-Vigh and Reglodi, 2004). PACAP has been shown to promote neurite outgrowth in PC12 cells and sympathetic neurons (Deutsch and Sun, 1992; DiCicco-Bloom *et al.*, 2000). In PC12D cells, PACAP activated Rac1 in a similar manner to dbcAMP (Supplemental Figure 5A). This Rac1 activation in response to PACAP treatment was completely abolished in STEF-depleted cells.

Depletion of STEF, but not Tiam1, attenuates dbcAMP-induced neurite outgrowth

Next we investigated dbcAMP-induced formation of mature neurites in knockdown cells. PC12D cells transfected with an empty pSUPER vector developed neurites within 48 h after dbcAMP addition (Figure 5A, top left). In contrast, depletion of STEF strongly inhibited neurite outgrowth (Figure 5A, top right). The proportions of neurite-bearing cells were calculated in control and knockdown cells (Figure 5B). In control cells, the proportion of neurite-bearing cells was 51% in the presence of dbcAMP. Only 22% of STEF knockdown cells bore neurites even in the presence of dbcAMP, however; this finding is consistent with the complete inhibition of dbcAMP-induced Rac1 activation in STEF-depleted cells (Figure 4). In Tiam1-depleted or Vav2/Vav3-depleted cells, no decrease in the proportion of neurite-bearing cells was observed in comparison with the control. The significant decrease in neurite outgrowth by STEF depletion was also observed in PACAP-treated PC12D cells (Supplemental Figure 5B). Together with the results shown in Figure 4, we concluded that STEF is the GEF most likely responsible for dbcAMP-induced Rac1 activation and that it plays a critical role in neurite outgrowth following dbcAMP treatment in PC12D cells.

PKA phosphorylates STEF

On the basis of the critical role of PKA and STEF in dbcAMP-induced Rac1 activation, we examined whether PKA directly phosphorylates STEF. Figure 6A shows that ΔN-STEF (Matsuo *et al.*, 2002) was efficiently phosphorylated by PKA in vitro; the amount of ΔN-STEF phosphorylation by PKA was comparable to that of PKA-phosphorylated βPix, the phosphorylation of which was reported previously (Chahdi *et al.*, 2005). Analysis of the primary sequence of STEF revealed Thr-749, Ser-782, and Ser-1562 as potential PKA phosphorylation sites (Figure 6B). Substitution of Thr-749, Ser-782, or Ser-1562 to Ala reproducibly reduced phosphorylation as compared with ΔN-STEF. The level of phosphorylation of triple mutant 3A (Thr-749A/Ser-782A/Ser-1562A) was only 16% of that of the original ΔN-STEF (Figure 6C). Thus Thr-749, Ser-782, and Ser-1562 are major phosphorylation sites by PKA in vitro. Furthermore, we tested whether STEF is phosphorylated by PKA in dbcAMP-treated cells. The dbcAMP-induced STEF phosphorylation proceeded gradually, and the level of STEF phosphorylation by PKA 30 min after dbcAMP addition was increased threefold compared with that in untreated cells (Figure 6D).

dbcAMP-induced Rac1 activation and neurite outgrowth are dependent on Thr-749 phosphorylation

Next we investigated which PKA phosphorylation site on STEF is important for dbcAMP-induced Rac1 activation. PC12D cells were transfected with a plasmid encoding wild-type STEF, Thr-749A, Ser-782A, Ser-1562A, or 3A STEF mutant, which is resistant to

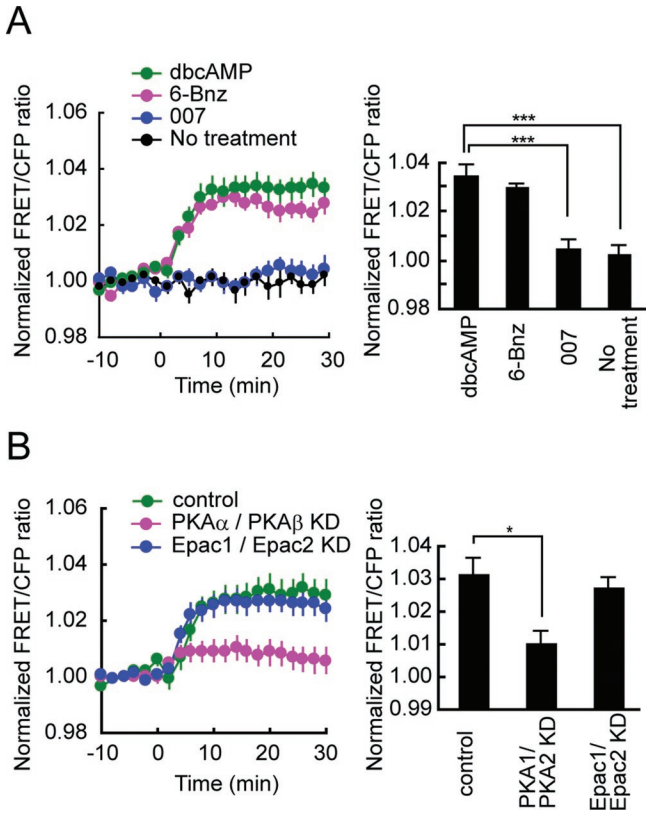

FIGURE 3: Comparison between PKA and Epac in the contribution to dbcAMP-induced Rac1 activation. (A) PC12D cells expressing Raichu-Rac1 were starved for 2 h and then mock-treated or treated with 1 mM dbcAMP, 100 μM 6-Bnz-cAMP, or 100 μM 007. Images were obtained every 2 min for 30 min after drug treatment. The number of experiments was as follows: dbcAMP (n = 20), 6-Bnz-cAMP (n = 12), 007 (n = 14), mock-treated (n = 10). Left, the mean FRET/CFP ratios averaged over the whole cell are expressed as in the legend to Figure 1B. Error bars show the SE. Right, the bar graph represents the average of the highest values of Rac1 activation in the indicated samples with SE. The symbols indicate the results of a Student's *t*-test analysis (***p < 0.001). (B) PC12D cells were transfected with an empty pSUPER vector, both pSUPER-PRKACA and pSUPER-PRKACB, or both Epac1 and Epac2. After selection with puromycin, the cells were further transfected with pRaichu-Rac1. After starvation for 2 h, images were obtained every 2 min for 30 min after dbcAMP addition. The number of experiments was as follows: control (n = 18), PRKACA and PRKACB KD (n = 13), Epac1/Epac2 KD (n = 16). Left, the mean FRET/CFP ratios averaged over the whole cell are expressed as in the legend to Figure 1B. Error bars show the SE. Right, the bar graph represents the average of the highest values of Rac1 activation in the indicated samples, with SE. The symbol indicates the result of a Student's *t* test (*p < 0.05).

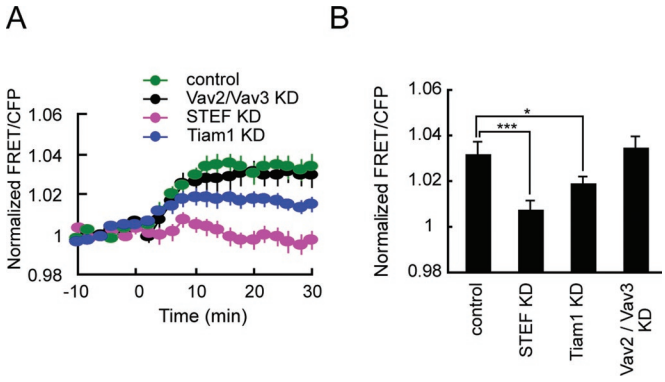

FIGURE 4: Effect of depletion of STEF, Tiam1, or Vav2/Vav3 on dbcAMP-induced Rac1 activation. PC12D cells were transfected with an empty pSUPER vector, pSUPER-STEF, pSUPER-Tiam1, or both pSUPER-Vav2 and pSUPER-Vav3. After selection with puromycin, the cells were further transfected with pRaichu-Rac1. After starvation for 2 h, images were obtained every 2 min for 30 min after dbcAMP addition. The number of experiments is as follows: control (n = 18), STEF KD (n = 12), Tiam1 KD (n = 12), Vav2/Vav3 KD (n = 20). (A) The mean FRET/CFP ratios averaged over the whole cell are expressed as in the legend to Figure 1B. Error bars show SE. (B) A bar graph represents the average of the highest values of Rac1 activation in the indicated samples with SE. The symbols indicate the results of a Student's *t* test (*p < 0.05; ***p < 0.001).

STEF shRNA in combination with pSUPER-STEF. After selection with puromycin, the cells were further transfected with pRaichu-Rac1 and subjected to FRET imaging (Figure 7A). Expression of shRNA-resistant wild-type STEF restored Rac1 activation. A large decrease in dbcAMP-induced Rac1 activation was observed in Thr-749A- and 3A-expressing cells. We observed no significant decrease in Rac1 activation in Ser-782A– or Ser-1562A–expressing cells.

The essential role of Thr-749 phosphorylation in dbcAMP-induced Rac1 activation was confirmed by the ectopic expression of STEF mutants in COS-7 cells, which express a negligible level of STEF protein. In mock-transfected COS-7 cells, we did not observe Rac1 activation following dbcAMP treatment (Figure 7B). In wild-type STEF-expressing cells, a significant increase in Rac1 activity after dbcAMP addition was detected. This STEF-mediated activation of Rac1 was decreased significantly by PKA depletion (Supplemental Figure 6A). This decrease is consistent with the prominent reduction of the level of dbcAMP-induced STEF phosphorylation in PKA-depleted cells (Supplemental Figure 6B). In this condition, mutation of Thr-749A, but not Ser-782A or Ser-1562A, completely abolished the STEF-dependent Rac1 activation in dbcAMP-treated cells. This suggests that Thr-749 phosphorylation by PKA could enhance GEF activity of STEF.

These results prompted us to examine the effect of point mutations in the PKA phosphorylation sites on STEF on dbcAMP-induced neurite outgrowth. As shown in Figure 7C, the expression of shRNA-resistant wild-type STEF restored neurite outgrowth following dbcAMP addition. As expected, a significant decrease in the proportion of neurite-bearing cells was observed in Thr-749A and 3A–expressing cells. The proportion of neurite-bearing cells in Ser-782A– or Ser-1562A–expressing cells was comparable to that in wild-type STEF-expressing cells. In conclusion, Thr-749 phosphorylation by PKA is critical for dbcAMP-induced Rac1 activation and neurite outgrowth.

PKA activity at the plasma membrane becomes localized to the neurite tips during dbcAMP-induced neurite outgrowth

One possible explanation for the local Rac1 activation in dbcAMP-induced neurite tips (Figure 1C) was localized PKA activity in proximity to the plasma membrane of the same neurite tips, because STEF has been shown to distribute throughout neuronal cells, including axon tips (Nishimura *et al*., 2005). We examined this possibility using the membrane-targeted PKA biosensor pm-AKAR3 (Allen and Zhang, 2006). PKA activity at the plasma membrane increased globally 30 min after dbcAMP addition; thereafter it gradually converged to the neurite tips (Figure 8A). This localization was more clearly observed in PC12D cells 1 d after dbcAMP addition (Figure 8B, top).

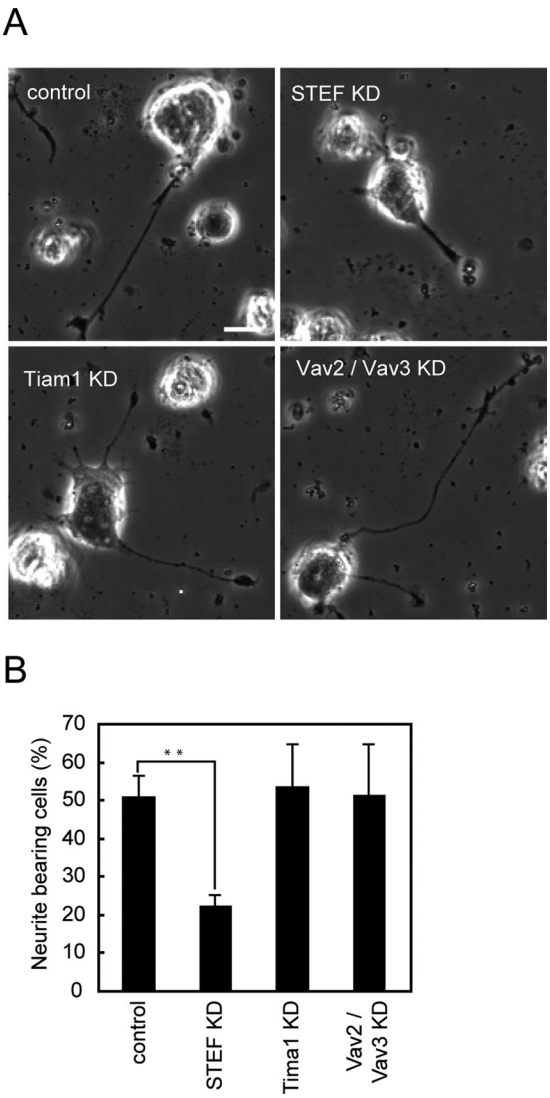

FIGURE 5: Effect of depletion of STEF, Tiam1, or Vav2/Vav3 on dbcAMP-induced neurite outgrowth. PC12D cells were transfected with an empty pSUPER vector, pSUPER-STEF, pSUPER-Tiam1, or both pSUPER-Vav2 and pSUPER-Vav3. After recovery, the cells were incubated with puromycin for 2 d. Then the selected cells were cultured with dbcAMP for 2 d and fixed for microscopy. At least 50 cells were assessed in each experiment, and the experiments were repeated three times. (A) Representative phase-contrast images of the control cells (top left), STEF-depleted cells (top right), Tiam1-depleted cells (bottom left), and Vav2/Vav3-depleted cells (bottom right). Bars, 10 μm. (B) Cells with neurites the lengths of which were at least twofold longer than their cell body lengths were scored as neurite-bearing cells. The results are expressed as the mean percentage of neurite-bearing cells with SE. The symbol indicates the result of a Student's *t* test; $^{**}p < 0.01$ compared with the control.

We quantified the localization of PKA activity using line-scanned data and linear fitting. The dbcAMP-induced neurite tips, but not the NGF-induced tips, showed a significant positive gradient of PKA activity (Figure 8B, bottom). These data indicate that localized PKA activation in the proximity of the plasma membrane of neurite tips could contribute to local Rac1 activation in the same neurite tips.

DISCUSSION

Here we have shown that phosphorylation of STEF by PKA is critical for Rac1 activation and neurite outgrowth in dbcAMP-treated PC12D cells. This is supported by our findings that knockdown of the catalytic subunits of PKA markedly reduced dbcAMP-induced Rac1 activation and that depletion of STEF abolished dbcAMP-induced Rac1 activation and neurite extension. PKA was able to phosphorylate STEF at three residues (Thr-749, Ser-782, Ser-1562) in vitro, among which Thr-749 was critical for dbcAMP-induced Rac1 activation and neurite extension. Our finding agrees with a previous report that dbcAMP-induced neurite outgrowth in PC12D cells was independent of PI3-kinase (Jin *et al.*, 2007) and argues against the idea that PI3-kinase signaling generally controls axon morphogenesis through the regulation of the cytoskeleton by Rho GTPases (Cosker and Eickholt, 2007; von Philipsborn and Bastmeyer, 2007).

Experiments using PKA- or Epac-specific cAMP analogues have shown that cAMP-induced neurite outgrowth in PC12 cells is mediated by both PKA and Epac (Christensen *et al.*, 2003; Kiermayer *et al.*, 2005); we confirmed these results in PC12D cells (unpublished data). However, the roles played by each continue to be a matter for debate (Cai *et al.*, 2001; Bouchard *et al.*, 2004; Aglah *et al.*, 2008; Murray and Shewan, 2008). Interconnectivity between the PKA- and Epac-signaling pathways (Bos, 2006) adds more complexity to this issue. The reported mechanisms underlying the contribution of PKA to neurite outgrowth are Erk1/2 activation through the Ca^{2+}-induced Rap1/B-Raf pathway (Vossler *et al.*, 1997; Zanassi *et al.*, 2001), cAMP response element-binding activation (Jessen *et al.*, 2001), and synapsin phosphorylation (Kao *et al.*, 2002). Considering the critical role of Rac1 in neurite outgrowth (Govek *et al.*, 2005; Hall and Lalli, 2010), the Rac1 activation by PKA-phosphorylated STEF shown in this study strongly suggests that the relative contributions of PKA and Epac in cAMP-induced neurite outgrowth must be reconsidered.

cAMP also plays a pivotal role in axon guidance in vitro (Piper *et al.*, 2007) and in vivo (Imai *et al.*, 2006). In vitro data are derived mainly from growth cone turning assays (Lohof *et al.*, 1992), which are based on the dichotomy between axon growth and guidance. A recent analysis of axon guidance in three-dimensional collagen gels (Mortimer *et al.*, 2010) has proposed, however, that growth-rate modulation, but not biased turning, dominates in shallow gradients, which might be similar to physiological situations. Thus the regulation of neurite outgrowth might be implicated in axonal chemotaxis under certain circumstances. Furthermore, the importance of Rac1 in axon guidance in the telencephalon has been demonstrated by studies using a conditional knockout of Rac1 (Chen *et al.*, 2007). Thus it is possible that Rac1 activation by PKA-phosphorylated STEF contributes to axon guidance using cAMP signals.

We suppose that localized PKA activation in the proximity of the plasma membrane of neurite tips leads to local Rac1 activation in the same neurite tips. Supplemental Figure 7, A and C, demonstrates that PKA and Rac1 were globally activated immediately after dbcAMP addition and subsequently inactivated throughout the cells at approximately 1.5–3 h (Supplemental Figure 8); thereafter the local activation appeared in parallel at neurite tips after 3–5 h. The local PKA activation near the plasma membrane of neurite tips is similar to the result in the recent report, in which membrane-associated PKA activity was highest at the leading edge in migrating CHO cells (Lim *et al.*, 2008). In addition, in fibroblasts undergoing chemotaxis, PKA activity was enriched in growing pseudopodia (Howe *et al.*, 2005). In both CHO cells and fibroblasts, polarized PKA activation was mediated by A kinase anchoring proteins (AKAPs). The connection between AKAPs and the cytoskeleton is thought to be important for cell migration (Diviani and Scott, 2001). In fact, many AKAPs, including AKAP-Lbc, ezrin, and WAVE-1, are linked to the actin cytoskeleton (Howe, 2004). Thus it is plausible that local PKA

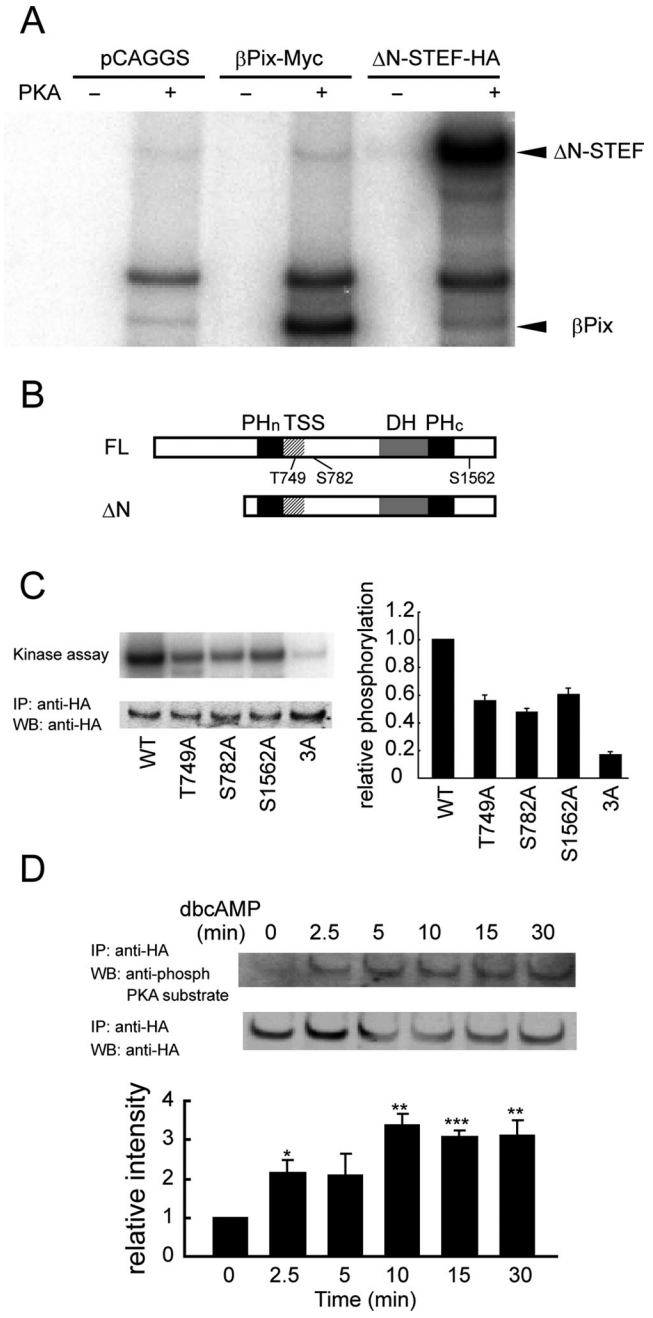

FIGURE 6: In vitro phosphorylation of STEF by PKA and in vivo phosphorylation of STEF following dbcAMP treatment. (A) COS-7 cells transfected with an empty pCAGGS vector, βPix-Myc–expressing plasmid, or ΔN-STEF-HA–expressing plasmid, incubated for 2 d, and lysed for immunoprecipitation with anti-HA (control and ΔN-STEF-HA) or anti-myc (βPix-Myc) antibody. The precipitated proteins were subjected to in vitro phosphorylation by PKA catalytic subunits with [γ-^{32}P]ATP in the kinase buffer. The phosphorylated products were resolved by SDS–PAGE and subjected to autoradiography. Arrowheads represent the positions of ΔN-STEF and βPix, respectively. (B) Diagrams of full-length (FL) and ΔN mutant of STEF. PHn, N-terminal pleckstrin homology; DH, Dbl homology; PHc, C-terminal pleckstrin homology. (C) cDNA encoding ΔN-STEF-HA or its mutants was transfected into COS-7 cells. In vitro kinase assays were performed as in (A). Experiments were repeated three times. Left, representative result. Top, an autoradiogram of phosphorylated ΔN-STEF-HA or its mutants. Bottom, an immunoblot with anti-HA antibody on anti-HA immunoprecipitates. Right, the averages of the relative levels of STEF phosphorylation in the indicated samples, with SE. (D) PC12D cells expressing full-length STEF were treated with dbcAMP for the indicated times and lysed for immunoprecipitation. Top, anti-HA immunoprecipitates were probed with anti-phospho PKA substrate or anti-HA antibody. Bottom, the averages of the relative levels of STEF phosphorylated by PKA, with SE (n = 3). The level of STEF phosphorylation in untreated cells was set to 1. The symbol indicates the result of a Student's *t* test (*p < 0.05; **p < 0.01; ***p < 0.001).

activity near the plasma membrane of dbcAMP-induced neurite tips reflects enrichment of PKA at the plasma membrane of neurite tips via particular AKAPs. Furthermore, the clear contrast between the immediate increase in PKA activity following dbcAMP addition (Supplemental Figure 2) and the gradual increase in STEF phosphorylation in dbcAMP-treated cells (Figure 6D) suggests that an additional process, such as the interaction between PKA and AKAPs, is required for dbcAMP-induced STEF phosphorylation. The different kinetics between PKA activity and STEF phosphorylation could explain the slight difference of the time-course between PKA activity and Rac1 activity after dbcAMP addition (shown in Supplemental Figure 8).

Tiam1 and STEF, both of which are highly expressed in neuronal tissues (Habets *et al.*, 1994; Hoshino *et al.*, 1999), are reported to have highly overlapping functions. Tiam1 and STEF are required for neurite outgrowth in N1E-115 cells as well as hippocampal neurons (Matsuo *et al.*, 2003). The introduction of dominant-negative forms of Tiam1 and STEF into the developing cerebral cortex revealed their pivotal role in neuronal migration (Kawauchi *et al.*, 2003). In contrast, this study showed that depletion of STEF, but not Tiam1, potently inhibited dbcAMP-induced neurite outgrowth; as far as we know, this is the first report of a STEF-specific function. The in vivo role of STEF during neuronal development and regeneration depending on cAMP signals should be an important issue in future studies.

How does the phosphorylation of Thr-749 on STEF increase its GEF activity for Rac1? Similarly to Tiam1, N-terminal truncation of STEF enhances its GEF activity, suggesting that the N-terminal autoinhibitory effect has to be removed for STEF activation to occur (Matsuo *et al.*, 2002). Four possible mechanisms can be considered: 1) Thr-749 phosphorylation may induce a conformational change in STEF, leading to an increase in its GEF activity. In the case of Tiam1, phosphorylation by Ca^{2+}/calmodulin-dependent kinase II is able to stimulate C1199-Tiam1-induced nucleotide exchange (Fleming *et al.*, 1999). 2) The binding of Par3 to the Tiam1-SIF-STEF homology (TSS) domain of STEF has been shown to activate STEF (Nishimura *et al.*, 2005). Thr-749 is located at the C terminus of the TSS domain. Thus Thr-749 phosphorylation may enhance the binding of Par3 to STEF, leading to an increase in its GEF activity. 3) PI3-kinase activity has been implicated in the control of Tiam1-driven activation of Rac1, probably through its effect on the membrane translocation of Tiam1 via the binding of PIP_3 to the TSS domain, including the N-terminal pleckstrin homology domain (Mertens *et al.*, 2003). The TSS domain of STEF exhibits a twofold higher affinity for PIP_3 than does the corresponding domain of Tiam1 (Terawaki *et al.*, 2010). Thus Thr-749 phosphorylation on STEF may enhance the binding of PIP_3 to its TSS domain, leading to membrane translocation and activation. 4) Like Tiam1, the binding of Rap1 to the TSS domain of STEF has been reported to mediate STEF-Rac1 signaling (Zaldua *et al.*, 2007). Thus Thr-749 phosphorylation may enhance the binding of Rap1 to STEF, leading to an

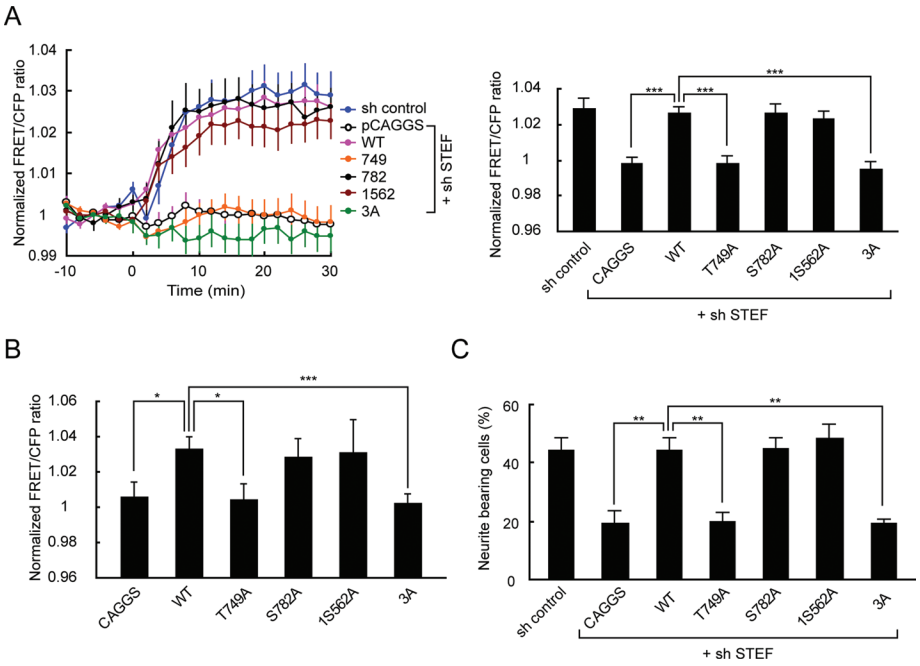

FIGURE 7: Identification of a critical PKA phosphorylation site on STEF for dbcAMP-induced Rac1 activation and neurite outgrowth. (A) PC12D cells were transfected with pCAGGS-3HA-resi-STEF-WT or its mutants in combination with pSUPER-STEF. After selection with puromycin, the cells were further transfected with pRaichu-Rac1. After starvation for 2 h, images were obtained every 2 min for 30 min after dbcAMP treatment. Left, time-course of the mean FRET/CFP ratios averaged over the whole cell. The number of experiments was as follows: control (n = 18), pCAGGS (n = 28), WT (n = 33), Thr-749A (n = 36), Ser-782A (n = 19), Ser-1562A (n = 18), 3A (n = 17). Error bars show the SE. Right, the bar graph represents the average of the highest values of Rac1 activation in the indicated samples, with SE. The symbols indicate the results of a Student's *t* test (***p < 0.001). (B) COS-7 cells were transfected with pCAGGS-3HA-resi-STEF-WT or its mutants in combination with pRaichu-Rac1. After starvation for 2 h, images were obtained every 2 min for 30 min after dbcAMP treatment. The bar graph represents the average of the highest values of the normalized FRET/CFP ratios during the 30 min in the indicated samples, with SE. The number of experiments was as follows: pCAGGS (n = 30), WT (n = 49), Thr-749A (n = 15), Ser-782A (n = 9), Ser-1562A (n = 16), 3A (n = 13). The symbols indicate the results of a Student's *t* test (*p < 0.05, ***p < 0.001). (C) PC12D cells were transfected with pCAGGS-3HA-resi-STEF-WT or its mutants in combination with pSUPER-STEF. After recovery, the cells were incubated with puromycin for 2 d, and then fixed for microscopy. Cells with neurites the lengths of which were at least twofold longer than their cell body lengths were scored as neurite-bearing cells. At least 50 cells were assessed in each experiment, and the experiments were repeated three times. The results are expressed as the mean percentage of neurite-bearing cells, with SE. The symbols indicate the results of a Student's *t* test (**p < 0.01).

increase in its GEF activity. The latter two possibilities seem unlikely, because a PI3-kinase inhibitor did not inhibit dbcAMP-induced Rac1 activation (Supplemental Figure 1A) and because depletion of Epac did not show any significant effect on Rac1 activation following dbcAMP addition (Figure 3B). Thus the former two possibilities will be subjects of future research. Because Thr-749 on STEF corresponds to Thr-679 on Tiam1, which is a potential PKA phosphorylation site, it would be interesting to investigate whether Tiam1 is similarly phosphorylated and activated by PKA.

Our goal is to elucidate the common requirements for neuritogenesis by comparing this study on cAMP signaling to our previous work on NGF signaling (Aoki *et al.*, 2004, 2005, 2007). NGF promoted the cycling of a positive feedback loop composed of PI3-kinase, Vav2/Vav3, Rac1/Cdc42, and actin cytoskeleton at neurite tips (Aoki *et al.*, 2005). We suppose that the coexistence of the SHIP2-mediated negative feedback on PIP_3 (Aoki *et al.*, 2007) leads to the rapidly alternating outgrowth and retraction of NGF-induced neurite tips (Figure 2). In contrast, dbcAMP-induced Rac1 activation and neurite outgrowth were independent of PI3-kinase and were affected by PKA-mediated phosphorylation of STEF. Also, the inhibitory effect of CdGAP and the CRIB domain of N-WASP on neurite outgrowth was significant but rather weak (Supplemental Figure 7); this shows a clear contrast with a drastic effect of Cdc42 inhibition on NGF-induced neuritogenesis (Aoki *et al.*, 2004). Furthermore, dbcAMP-induced neurites extended continuously. Despite the substantial differences in signaling mechanisms and the mode of morphological changes, the local activation of Rac1 and Cdc42 at neurite tips is similar between NGF- and dbcAMP-treated cells. Rac1 and Cdc42 play a critical role in neurite outgrowth (Govek *et al.*, 2005; Hall and Lalli, 2010). Thus we propose that local activation of both Rac1 and Cdc42 at neurite tips is necessary for neurite outgrowth, which is crucial for the wiring of the developing nervous system.

MATERIALS AND METHODS

FRET biosensors

The plasmids encoding the FRET biosensors, Raichu-Rac1/1011x, Raichu-Cdc42/1054x (Itoh *et al.*, 2002), and Pippi-PIP_3 (Aoki *et al.*, 2005), have been described previously. pRaichu-Rac1/2246x was derived from pRaichu-Rac1/1011x and encodes a Rac1 biosensor with a broad dynamic range (N. Komatsu *et al.*, unpublished data). The plasmid encoding pmAKAR3 (Allen and Zhang, 2006) was provided by J. Zhang (Johns Hopkins University School of Medicine, Baltimore, MD).

Plasmid

The RNA targeting constructs were generated using pSUPER.retro.puro vector (OligoEngine, Seattle, WA). The 19- or 21-nucleotide sequences used to target rat PKA catalytic subunit α (PRKACA), rat PKA catalytic subunit β (PRKACB), Tiam1, and STEF mRNAs were: 5′-GTGGTTTGCCACAACTGAC-3′, 5′-GGTTGAGGCTCCATTCATACC-3′, 5′-GTCGGAAATCAAGAAGCTG-3′, and 5′-GGAGCTGCCTTTCTCACTTTA-3′, respectively. The 19-nucleotide sequences used to target rat Vav2 and Vav3 mRNAs have been described previously (Aoki *et al.*, 2005). The full-length mouse STEF cDNA (Hoshino *et al.*, 1999) was point-mutated to resist short-hairpin RNA (shRNA)-mediated knockdown and was subcloned into the pCAGGS-3HA vector (Aoki *et al.*, 2007) to generate pCAGGS-3HA-resi-STEF. Point mutations in pcDNA3-ΔN STEF (Matsuo *et al.*, 2002) and pCAGGS-3HA-resi-STEF were generated using a QuickChange II site-directed mutagenesis kit (Invitrogen, Carlsbad, CA). The cDNA for PRKACB was subcloned into the pCAGGS-3HA vector.

Cells, reagents, and antibodies

PC12D cells (a gift from M. Sano, Kyoto Prefectural University of Medicine, Kyoto, Japan), a subline of PC12 cells that extend neurites rapidly in response to dbcAMP (Katoh-Semba *et al.*, 1987), were maintained in DMEM supplemented with 10% horse

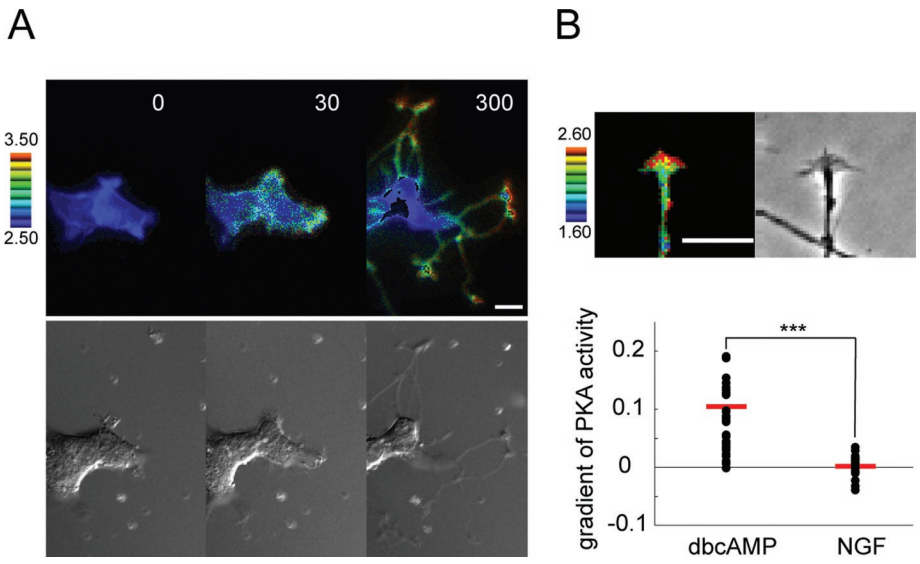

FIGURE 8: Spatiotemporal changes in PKA activity following dbcAMP treatment. (A) PC12D cells expressing pmAKAR3 were starved for 2 h and then treated with 1 mM dbcAMP. Images were obtained every 5 min for 300 min after dbcAMP addition (n = 12). Representative ratio images of FRET/CFP at the indicated time points (in min) after dbcAMP addition are shown as in the legend to Figure 1A. Bars, 10 μm. (B) PC12D cells expressing pmAKAR3 were incubated with 1 mM dbcAMP for 1 d, and then images were obtained every 2 min for 40 min. Top, a representative ratio image of FRET/CFP in neurite tips is shown. Bars, 10 μm. Bottom, distributions of gradients of PKA activity in dbcAMP- or NGF-induced neurite tips. Red bars represent averages.

serum and 5% fetal bovine serum. The cells were plated on 35-mm glass-base dishes (Asahi Techno Glass, Tokyo, Japan) coated with polyethyleneimine (Sigma-Aldrich, St. Louis, MO). COS-7 and HeLa cells were maintained in DMEM containing 10% fetal bovine serum. dbcAMP and NGF were purchased from Calbiochem (La Jolla, CA). Puromycin and N^6-benzoyladenosine-3′,5′-cyclical monophosphate (6-Bnz-cAMP) were obtained from Sigma-Aldrich. 8-para-chloro-phenyl-thio-2′-O-methyl-cAMP (007) was obtained from Tocris Cookson (Ballwin, MO). Anti-myc (9E10) monoclonal antibody was purchased from Santa Cruz Biotechnology (Santa Cruz, CA). Phospho-(Ser/Thr) PKA substrate antibody was obtained from Cell Signaling Technology (Beverly, MA). Anti-HA monoclonal antibody was obtained from Roche Diagnostics (Indianapolis, IN).

RNA interference experiments

PC12D cells were transfected with the desired pSUPER constructs by using Lipofectamine 2000 (Invitrogen). After recovery, the cells were selected by a 2-d incubation with 2 μg/ml puromycin and then used for further analysis. For FRET imaging, the indicated pRaichu plasmids were transfected into the shRNA-expressing cells 1 d after transfection of the pSUPER constructs. After an additional 2-d incubation with puromycin, the cells were starved and used for imaging.

Time-lapse imaging

PC12D or COS-7 cells expressing FRET biosensors were starved for 2 h with phenol red-free DMEM/F-12 medium (Invitrogen) containing 0.1% bovine serum albumin and then treated with cAMP analogues. The medium was covered with mineral oil (Sigma-Aldrich) to preclude evaporation. Cells were imaged with an IX81 inverted microscope (Olympus, Tokyo, Japan) equipped with a Cool SNAP-HQ cooled charge-coupled device camera (Roper Scientific, Trenton, NJ), a laser-based auto-focusing system (IX2-ZDC; Olympus), and an automatically programmable XY stage (MD-XY30100T-Meta; SIGMA KOKI, Tokyo, Japan), which allowed us to obtain time-lapse images of several fields of view in a single experiment. The following filters used for the dual-emission imaging were obtained from Omega Optical (Brattleboro, VT): an XF1071 (440AF21) excitation filter; an XF2034 (455DRLP) dichroic mirror; and two emission filters (XF3075 [480AF30] for CFP and XF3079 [535AF26] for FRET). Cells were illuminated with a 75-W Xenon lamp through a 12% neutral density filter and viewed through a 60× oil immersion objective lens (PlanApo 60×/1.4, Olympus). The exposure times for 4 × 4 binning were 500 ms for CFP and FRET images and 100 ms for phase-contrast images. After background subtraction, FRET/CFP ratio images were created with MetaMorph software (Universal Imaging, West Chester, PA), and the images were used to represent FRET efficiency.

Neurite outgrowth assay

PC12D cells were transfected with the indicated pSUPER constructs and selected with 2 μg/ml puromycin for 2 d. Then neurite outgrowth was induced with 1 mM dbcAMP and allowed to proceed for 48 h in DMEM/F-12 medium containing 0.1% bovine serum albumin and 2 μg/ml puromycin. Quantification of neurite outgrowth was performed as described previously (Nakamura *et al.*, 2002).

In vitro kinase assay

COS-7 cells were transfected with the indicated plasmids using 293fectin (Invitrogen). Two days after transfection, cells were harvested in ice-cold lysis buffer (25 mM Tris pH 7.5, 150 mM NaCl, 1.5 mM $MgCl_2$, 1% Nonidet P-40, 10% glycerol, 1 mM EDTA, 1 mM EGTA, 2 mM sodium orthovanadate, 50 mM sodium fluoride, 1 mM phenylmethylsulfonyl fluoride, and 10 μg/ml aprotinin). The cleared lysates were incubated with 3 μg of anti-myc antibody or 1 μg of anti-HA antibody. After 1.5-h tumbling at 4°C, protein G-Sepharose (GE Healthcare, Little Chalfont, UK) was added, and incubation was continued for 1 h at 4°C. After washing three times with ice-cold lysis buffer, the beads were washed once with kinase buffer (50 mM HEPES, pH 7.5, 10 mM $MgCl_2$, 1 mM EGTA, 1 mM dithiothreitol, 0.015% Tween 20), and suspended into 40 μl of kinase buffer. Then the immunoprecipitates were incubated with two units of PKA catalytic subunit (Sigma-Aldrich) and 740 kBq of [γ-^{32}P]ATP (111 Tbq/mmol; PerkinElmer, Waltham, MA) for 10 min at 30°C. After washing three times with kinase buffer, the beads were boiled in sample buffer, and the bound proteins were resolved by SDS–PAGE and subjected to autoradiography.

Immunoprecipitation

Cells were harvested in ice-cold lysis buffer. The cleared lysates were incubated with 1 μg of anti-HA antibody. After 30-min tumbling at 4°C, protein G-Sepharose was added and incubation was continued for 1 h at 4°C. The washed beads were boiled in sample buffer, and the bound proteins were analyzed by immunoblotting.

ACKNOWLEDGMENTS

We thank Akiko Abe, Rie Sakai, Yoshie Inaoka, Kyoko Hirano, Yasuko Kasakawa, and Natsuko Nonaka for technical assistance and members of the Matsuda Laboratory for their input. This work was supported by grants from the Ministry of Education, Culture, Sports, Science and Technology of Japan; the Cell Innovation Program and Innovate Techno-Hub for Integrated Medical Bio-imaging Project from MEXT; the Kyoto University Global COE Program Center for Frontier Medicine; the Uehara Memorial Foundation; the Research Foundation for Opto-Science and Technology; and the Naito Foundation and by a Sagawa Cancer Research Grant.

REFERENCES

Aglah C, Gordon T, Posse de Chaves EI (2008). cAMP promotes neurite outgrowth and extension through protein kinase A but independently of Erk activation in cultured rat motoneurons. Neuropharmacol 55, 8–17.

Allen MD, Zhang J (2006). Subcellular dynamics of protein kinase A activity visualized by FRET-based reporters. Biochem Biophys Res Commun 348, 716–721.

Aoki K, Nakamura T, Fujikawa K, Matsuda M (2005). Local phosphatidylinositol 3,4,5-trisphosphate accumulation recruits Vav2 and Vav3 to activate Rac1/Cdc42 and initiate neurite outgrowth in nerve growth factor-stimulated PC12 cells. Mol Biol Cell 16, 2207–2217.

Aoki K, Nakamura T, Inoue T, Meyer T, Matsuda M (2007). An essential role for the SHIP2-dependent negative feedback loop in neuritogenesis of nerve growth factor-stimulated PC12 cells. J Cell Biol 177, 817–827.

Aoki K, Nakamura T, Matsuda M (2004). Spatio-temporal regulation of Rac1 and Cdc42 activity during nerve growth factor-induced neurite outgrowth in PC12 cells. J Biol Chem 279, 713–719.

Bos JL (2006). Epac proteins: multi-purpose cAMP targets. Trends Biochem Sci 31, 680–686.

Bouchard JF, Moore SW, Tritsch NX, Roux PP, Shekarabi M, Barker PA, Kennedy TE (2004). Protein kinase A activation promotes plasma membrane insertion of DCC from an intracellular pool: A novel mechanism regulating commissural axon extension. J Neurosci 24, 3040–3050.

Cai D, Shen Y, De Bellard M, Tang S, Filbin MT (1999). Prior exposure to neurotrophins blocks inhibition of axonal regeneration by MAG and myelin via a cAMP-dependent mechanism. Neuron 22, 89–101.

Cai D, Qiu J, Cao Z, McAtee M, Bregman BS, Filbin MT (2001). Neuronal cyclic AMP controls the developmental loss in ability of axons to regenerate. J Neurosci 21, 4731–4739.

Chahdi A, Miller B, Sorokin A (2005). Endothelin 1 induces β_1Pix translocation and Cdc42 activation via protein kinase A-dependent pathway. J Biol Chem 280, 578–584.

Chakrabarti K, Lin R, Schiller NI, Wang Y, Koubi D, Fan YX, Rudkin BB, Johnson GR, Schiller MR (2005). Critical role for kalirin in nerve growth factor signaling through TrkA. Mol Cell Biol 25, 5106–5118.

Chen L, Liao G, Waclaw RR, Burns KA, Linquist D, Campbell K, Zheng Y, Kuan CY (2007). Rac1 controls the formation of midline commissures and the competency of tangential migration in ventral telencephalic neurons. J Neurosci 27, 3884–3893.

Christensen AE *et al.* (2003). cAMP analog mapping of Epac1 and cAMP kinase. Discriminating analogs demonstrate that Epac and cAMP kinase act synergistically to promote PC-12 cell neurite extension. J Biol Chem 278, 35394–35402.

Cosker KE, Eickholt BJ (2007). Phosphoinositide 3-kinase signalling events controlling axonal morphogenesis. Biochem Soc Trans 35, 207–210.

Cote JF, Vuori K (2007). GEF what? Dock180 and related proteins help Rac to polarize cells in new ways. Trends Cell Biol 17, 383–393.

Deutsch PJ, Sun Y (1992). The 38-amino acid form of pituitary adenylate cyclase-activating polypeptide stimulates dual signaling cascades in PC12 cells and promotes neurite outgrowth. J Biol Chem 267, 5108–5113.

DiCicco-Bloom E, Deutsch PJ, Maltzman J, Zhang J, Pintar JE, Zheng J, Friedman WF, Zhou X, Zaremba T (2000). Autocrine expression and ontogenetic functions of the PACAP ligand/receptor system during sympathetic development. Dev Biol 219, 197–213.

Diviani D, Scott JD (2001). AKAP signaling complexes at the cytoskeleton. J Cell Sci 114, 1431–1437.

Dong JM, Leung T, Manser E, Lim L (1998). cAMP-induced morphological changes are counteracted by the activated RhoA small GTPase and the Rho kinase ROKα. J Biol Chem 372, 26522–45522.

Enserink JM, Christensen AE, de Rooij J, van Triest M, Schwede F, Genieser HG, Doskeland SO, Blank JL, Bos JL (2002). A novel Epac-specific cAMP analogue demonstrates independent regulation of Rap1 and ERK. Nat Cell Biol 4, 901–906.

Fimia GM, Sassone-Corsi P (2001). Cyclic AMP signalling. J Cell Sci 114, 1971–1972.

Fleming IN, Elliott CM, Buchanan FG, Downes CP, Exton JH (1999). Ca^{2+}/calmodulin-dependent protein kinase II regulates Tiam1 by reversible protein phosphorylation. J Biol Chem 274, 12753–12758.

Govek EE, Newey SE, Van Aelst L (2005). The role of the Rho GTPases in neuronal development. Genes Dev 19, 1–49.

Habets GG, Scholtes EH, Zuydgeest D, Van Der Kammen RA, Stam JC, Berns A, Collard JG (1994). Identification of an invasion-inducing gene, Tiam-1, that encodes a protein with homology to GDP-GTP exchangers for Rho-like proteins. Cell 77, 537–549.

Hall A (1998). Rho GTPases and the actin cytoskeleton. Science 279, 509–514.

Hall A, Lalli G (2010). Rho and Ras GTPases in axon growth, guidance, and branching. Cold Spring Harb Perspect Biol 2, a001818.

Heasman SJ, Ridley AJ (2008). Mammalian Rho GTPases: new insights into their functions from in vivo studies. Nat Rev Mol Cell Biol 9, 690–701.

Hoshino M, Sone M, Fukata M, Kuroda S, Kaibuchi K, Nabeshima Y, Hama C (1999). Identification of the stef gene that encodes a novel guanine nucleotide exchange factor specific for Rac1. J Biol Chem 274, 17837–17844.

Howe AK (2004). Regulation of actin-based cell migration by cAMP/PKA. Biochim Biophys Acta 1692, 159–174.

Howe AK, Baldor LC, Hogan BP (2005). Spatial regulation of the cAMP-dependent protein kinase during chemotactic cell migration. Proc Natl Acad Sci USA 102, 14320–14325.

Imai T, Suzuki M, Sakano H (2006). Odorant receptor-derived cAMP signals direct axonal targeting. Science 314, 657–661.

Itoh RE, Kurokawa K, Ohba Y, Yoshizaki H, Mochizuki N, Matsuda M (2002). Activation of rac and cdc42 video imaged by fluorescent resonance energy transfer-based single-molecule probes in the membrane of living cells. Mol Cell Biol 22, 6582–6591.

Jessen U, Novitskaya V, Pedersen N, Serup P, Berezin V, Bock E (2001). The transcription factors CREB and c-Fos play key roles in NCAM-mediated neuritogenesis in PC12-E2 cells. J Neurochem 79, 1149–1160.

Jin E, Nosaka K, Sano M (2007). NGF-dependent formation of ruffles in PC12D cells required a different pathway from that for neurite outgrowth. Neurochem Int 51, 216–226.

Kao HT, Song HJ, Porton B, Ming GL, Hoh J, Abraham M, Czernik AJ, Pieribone VA, Poo MM, Greengard P (2002). A protein kinase A-dependent molecular switch in synapsins regulates neurite outgrowth. Nat Neurosci 5, 431–437.

Katoh H, Yasui H, Yamaguchi Y, Aoki J, Fujita H, Mori K, Negishi M (2000). Small GTPase RhoG is a key regulator for neurite outgrowth in PC12 cells. Mol Cell Biol 20, 7378–7387.

Katoh-Semba R, Kitajima S, Yamazaki Y, Sano M (1987). Neuritic growth from a new subline of PC12 pheochromocytoma cells: cyclic AMP mimics the action of nerve growth factor. J Neurosci Res 17, 36–44.

Kawauchi T, Chihama K, Nabeshima Y, Hoshino M (2003). The in vivo roles of STEF/Tiam1, Rac1 and JNK in cortical neuronal migration. EMBO J 22, 4190–4201.

Kiermayer S, Biondi RM, Imig J, Plotz G, Haupenthal J, Zeuzem S, Piiper A (2005). Epac activation converts cAMP from a proliferative into a differentiation signal in PC12 cells. Mol Biol Cell 16, 5639–5648.

Lim CJ, Kain KH, Tkachenko E, Goldfinger LE, Gutierrez E, Allen MD, Groisman A, Zhang J, Ginsberg MH (2008). Integrin-mediated protein kinase A activation at the leading edge of migrating cells. Mol Biol Cell 19, 4930–4941.

Lohof AM, Quillan M, Dan Y, Poo MM (1992). Asymmetric modulation of cytosolic cAMP activity induces growth cone turning. J Neurosci 12, 1253–1261.

Luo L (2000). Rho GTPases in neuronal morphogenesis. Nat Rev Neurosci 1, 173–180.

Matsuo N, Hoshino M, Yoshizawa M, Nabeshima Y (2002). Characterization of STEF, a guanine nucleotide exchange factor for Rac1, required for neurite growth. J Biol Chem 277, 2860.

Matsuo N, Terao M, Nabeshima Y, Hoshino M (2003). Roles of STEF/Tiam1, guanine nucleotide exchange factors for Rac1, in regulation of growth cone morphology. Mol Cell Neurosci 24, 69–81.

McPherson CE, Eipper BA, Mains RE (2002). Genomic organization and differential expression of Kalirin isoforms. Gene 284, 41–51.

Mertens AE, Roovers RC, Collard JG (2003). Regulation of Tiam1-Rac signalling. FEBS Lett 546, 11–16.
Miyawaki A (2003). Visualization of the spatial and temporal dynamics of intracellular signaling. Dev Cell 4, 295–305.
Mortimer D, Pujic Z, Vaughan T, Thompson AW, Feldner J, Vetter I, Goodhill GJ (2010). Axon guidance by growth-rate modulation. Proc Natl Acad Sci USA 107, 5202–5207.
Murray AJ, Shewan DA (2008). Epac mediates cyclic AMP-dependent axon growth, guidance and regeneration. Mol Cell Neurosci 38, 578–588.
Nakamura T, Komiya M, Sone K, Hirose E, Gotoh N, Morii H, Ohta Y, Mori N (2002). Grit, a GTPase-activating protein for the Rho family, regulates neurite extension through association with the TrkA receptor and N-Shc and CrkL/Crk adapter molecules. Mol Cell Biol 22, 8721–8734.
Nakamura T, Matsuda M (2009). In vivo imaging of signal transduction cascades with probes based on Förster resonance energy transfer (FRET). Curr Protoc Cell Biol Unit 14,10.
Neumann S, Bradke F, Tessier-Lavigne M, Basbaum AI (2002). Regeneration of sensory axons within the injured spinal cord induced by intraganglionic cAMP elevation. Neuron 34, 885–893.
Nishimura T, Yamaguchi T, Kato K, Yoshizawa M, Nabeshima Y, Ohno S, Hoshino M, Kaibuchi K (2005). PAR-6-PAR-3 mediates Cdc42-induced Rac activation through the Rac GEFs STEF/Tiam1. Nat Cell Biol 7, 270–277.
Piper M, van Horck F, Holt C (2007). The role of cyclic nucleotides in axon guidance. In: Axon Growth and Guidance, ed. D. Bagnard, New York: Landes Bioscience and Springer, 134–143.
Qiu J, Cai D, Dai H, McAtee M, Hoffman PN, Bregman BS, Filbin MT (2002). Spinal axon regeneration induced by elevation of cyclic AMP. Neuron 34, 895–903.
Richter-Landsberg C, Jastorff B (1986). The role of cAMP in nerve growth factor-promoted neurite outgrowth in PC12 cells. J Cell Biol 102, 821–829.
Rydel RE, Greene LA (1988). cAMP analogs promote survival and neurite outgrowth in cultures of rat sympathetic and sensory neurons independently of nerve growth factor. Proc Natl Acad Sci USA 85, 1257–1261.
Somogyvari-Vigh A, Reglodi D (2004). Pituitary adenylate cyclase activating polypeptide: a potential neuroprotective peptide. Curr Pharm Des 10, 2861–2889.
Song H, Ming G, He Z, Lehmann M, McKerracher L, Tessier-Lavigne M, Poo M (1998). Conversion of neuronal growth cone responses from repulsion to attraction by cyclic nucleotides. Science 281, 1515–1518.
Terawaki S, Kitano K, Mori T, Zhai Y, Higuchi Y, Itoh N, Watanabe T, Kaibuchi K, Hakoshima T (2010). The PHCCEx domain of Tiam1/2 is a novel protein- and membrane-binding module. EMBO J 29, 236–250.
Van Aelst L, D'Souza-Schorey C (1997). Rho GTPases and signaling networks. Genes Dev 11, 2295–2322.
von Philipsborn A, Bastmeyer M (2007). Mechanisms of gradient detection: a comparison of axon pathfinding with eukaryotic cell migration. Int Rev Cytol 263, 1–62.
Vossler MR, Yao H, York RD, Pan MG, Rim CS, Stork PJ (1997). cAMP activates MAP kinase and Elk-1 through a B-Raf- and Rap1-dependent pathway. Cell 89, 73–82.
Zaldua N, Gastineau M, Hoshino M, Lezoualc'h F, Zugaza JL (2007). Epac signaling pathway involves STEF, a guanine nucleotide exchange factor for Rac, to regulate APP processing. FEBS Lett 581, 5814–5818.
Zanassi P, Paolillo M, Feliciello A, Avvedimento EV, Gallo V, Schinelli S (2001). cAMP-dependent protein kinase induces cAMP-response element-binding protein phosphorylation via an intracellular calcium release/ERK-dependent pathway in striatal neurons. J Biol Chem 276, 11487–11495.
Zheng JQ, Zheng Z, Poo M (1994). Long-range signaling in growing neurons after local elevation of cyclic AMP-dependent activity. J Cell Biol 127, 1693–1701.